

## Chapter 2

# Seismic Precursors to Volcanic Explosions During the 2006 Eruption of Augustine Volcano

By Helena Buurman<sup>1</sup> and Michael E. West<sup>1</sup>

### Abstract

The 2006 eruption of Augustine Volcano, Alaska, generated more than 3,500 earthquakes in a month-long time frame bracketing the most explosive period of activity. We examine two quantitative tools that, in retrospective analysis, were excellent indicators of imminent eruption. The first tool, referred to as the frequency index (*FI*), is based on a simple ratio of high- and low-frequency energy in an earthquake seismogram. It is a metric that allows us to quantify the differences between the canonical high-frequency, hybrid, and low-frequency volcanic earthquakes. *FI* values greater than  $-0.4$  indicate earthquakes classically referred to as high-frequency or volcano-tectonic events. *FI* values less than  $-1.3$  correspond to events usually referred to as low-frequency earthquakes. Because the *FI* is based on a ratio and not a spectral peak, hybrid earthquakes are successfully assigned *FI* values intermediate to these two classes. In this eruption, we find a remarkable correlation between events with *FI* less than  $-1.8$  and explosive eruptions. The second tool we examine is based on repeating seismic waveforms identified through waveform cross-correlation. Although the vast majority of earthquakes during this eruption have unique waveforms, subsets of events exhibiting a high degree of similarity occur and are closely tied to explosive eruption events. Of the 13 large explosion events, seven were preceded by clusters of highly similar earthquakes. We apply the *FI* and correlation tools together to identify changes in high- and low-frequency earthquake occurrences and examine their relations to the precursory, explosive, and continuous phases of the eruption. We find that earthquakes that have low *FI* values and earthquakes exhibiting high degrees of similarity occur almost exclusively within hours of explosive eruptions and postulate

that they occur as a result of the final ascent of magma in the volcanic edifice. Because neither of these methods requires analyst-reviewed earthquake locations, we believe that they have considerable potential as automated real-time volcano monitoring tools.

### Introduction

Seismicity has long been one of the most commonly monitored aspects of active volcanoes. Different volcanic processes produce very different types of earthquakes, varying in waveform duration, onset, frequency content, and amplitude. Earthquakes with impulsive P and S arrivals and peak frequencies between 5 and 15 Hz, for example, are typically the result of brittle failure of rock within the volcanic edifice (McNutt, 1996). They often occur at high rates during episodes of volcanic unrest, although they are also part of the natural background seismicity found at volcanoes. Another type of earthquake routinely observed during episodes of volcanic activity has an emergent P arrival and often lacks a distinct S arrival. This type of earthquake is dominated by frequencies between 1 and 5 Hz, has little energy at frequencies greater than 15 Hz, and is thought to result from the resonance of fluid-filled cracks (Chouet, 1988). Numerous trigger mechanisms exist for such a process, and we refer to the summaries of Neuberg and others (2005) and Petersen (2007) for excellent overviews.

Certain volcanic processes can cause earthquakes to have remarkably similar waveform characteristics. For one waveform to appear the same as another it must originate in approximately the same place and from the same process. Nondestructive processes such as stick-slip movement along a fault or conduit or destructive mechanisms such as the incremental opening of cracks are possible sources for such earthquakes. The low-frequency resonant sources can be particularly rich in similar waveforms because of their inherently nondestructive source (for example, Stephens and Chouet, 2001; Petersen, 2007).

Perhaps the most basic metric for tracking volcanic seismicity is the overall rate of earthquakes. Eruptions are

---

<sup>1</sup>Alaska Volcano Observatory, Geophysical Institute, University of Alaska Fairbanks, 903 Koyukuk Drive, Fairbanks, AK 99775.

almost always preceded by some type of earthquake swarm. The swarm may last hours or months and may contain a variety of earthquake types or consist of just one style of event (Benoit and McNutt, 1996). The wide range of swarm characteristics reflects the wide range of processes thought to produce them. However, the nearly ubiquitous existence of precursory seismic swarms is one of the foundations of volcano monitoring.

Quantifying seismic activity is an effective method for inferring the level of unrest and the type of activity occurring at a volcano. This can be challenging in a real-time setting because the rate of seismic activity in a precursory swarm typically exceeds the rate at which events can be processed by any sort of analyst-reviewed process. Earthquakes are often classified manually, and this is usually based on the experience and interpretation of the analyst in subjective method that can lead to inconsistencies across or even within datasets (Langer and others, 2006). The manual review of earthquakes is impossible to accomplish in real time during rapid seismic sequences, even though assessing earthquake parameters such as frequency content is precisely what is needed in order to know whether or not such swarms are building towards an eruption.

We present a method for differentiating between earthquake types based on their frequency content. Our approach is simple and can be applied without user intervention. We apply this method to the explosive sequences of the 2006

eruption of Augustine Volcano, Alaska. The method is largely independent of earthquake locations and is robust to changes in seismic network coverage. The only assumption we make is that the seismic events are being generated by the volcano—a reasonable assumption given the high rates of seismicity during most eruptions. This is particularly relevant to Augustine, where the earthquakes are clustered together such that the first-order earthquake locations (which at some volcanoes exhibit a clear rise to the surface before eruption; for example, Harlow and others, 1994) provided limited information about the eruptive processes.

We also investigate patterns of repeating earthquakes and examine how they relate to eruptive behavior. The classification of seismic events combined with the identification of repeating earthquakes provides a different insight into the processes that occur at an erupting volcano. We show that an automated analysis of this type could provide key observations and even identify precursors to explosive activity.

## Augustine Volcano

Augustine Volcano is a 10-km-wide island located in Cook Inlet between the Kenai Peninsula and Cape Douglas, 115 km from the town of Homer, in south-central Alaska. It has an historical eruptive history dating back to 1812 and erupted four

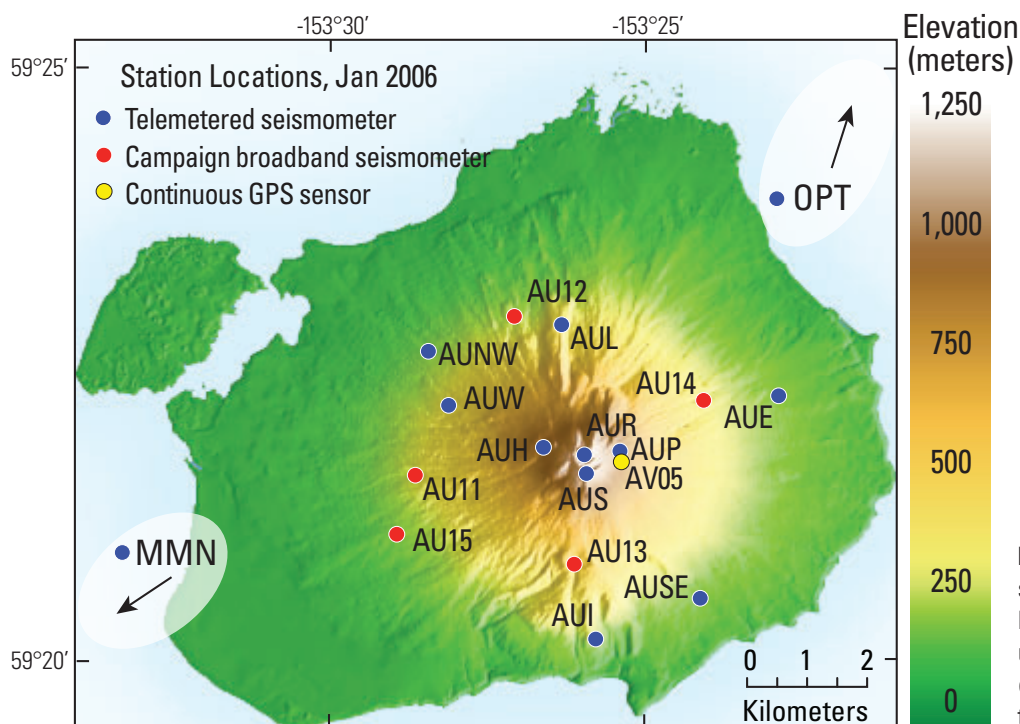


**Figure 1.** Locations of seismic stations on Augustine Island. Reference stations MMN and OPT used during the compilation of the catalog are located on the mainland; their directions are indicated.

times in the twentieth century alone, with the most recent eruption occurring in 1986 (Power and Lalla, this volume).

The 2006 eruption of Augustine began on January 11, following an 8.5-month period of precursory seismic activity (Jacobs and McNutt, this volume; Power and Lalla, this volume). An earthquake swarm occurred on January 10–11, 2006, which culminated in two phreatic explosions (Wallace and others, this volume) and heralded the onset of the explosive eruption sequence. On the basis of the character of unrest and the resultant eruptive deposits, Coombs and others (this volume) divide the eruption into several different phases. The explosive phase occurred between January 11 and January 28, during which time the eruptive activity was characterized by 2 largely phreatic and 11 magmatic explosions that generated ash plumes to heights greater than 9 km above sea level (asl) (Bailey and others, this volume), with repose periods between events lasting hours to days. These events recorded peak amplitudes greater than 20 Pa on the local pressure sensor located at station AUE (fig. 1), 3.5 km east of the volcano's summit. The explosions in the latter half of January were also strong enough to be recorded on the 153US infrasonic array at Fairbanks, 675 km north of Augustine (Wilson and others, 2006). A period of continuous eruptive activity (the continuous phase) began on January 28. This was characterized by a persistent ash plume up to 5 km asl (Bailey and others, this volume), produced by discrete but frequent (minutes to hours apart) minor explosions measuring less than 20 Pa at pressure sensor AUE. A gradual transition to effusive behavior followed, in which the small explosive events became fewer in number during the first week of February and the eruptive activity became dominated by dome growth with associated rockfalls and block and ash flows. Finally, a period of dome growth and lava flow (the effusive phase) between March 3 and March 16 brought the 2006 eruption sequence to a close.

The dataset used in this study spans the last 11 days of the precursory phase, which terminates with a vigorous seismic swarm of over 780 earthquakes, the entire explosive phase from January 11 to January 28, and the majority of the continuous phase from January 28 to February 6. By February 6 the seismic activity had begun to wane considerably and the volcano was moderately quiet until a short effusive dome-building phase occurred in early March 2006.

## Data

Augustine was one of the more densely instrumented volcanoes in Alaska before 2006 as a result of its recent eruptive history and its proximity to settlements. The real-time seismic network on the island consisted of 10 short-period seismic stations at distances between 0 and 3.5 km from the summit and a broad-band seismometer 2.5 km from the summit. In late December 2005 the Alaska Volcano Observatory (AVO) deployed five campaign broad-band seismometers with on-site recording, as well as a telemetered strong motion sensor at a distance of 4.5 km. Over the course of the eruption, the five telemetered seismometers closest to the summit were

destroyed, along with broad-band seismometer AU12. The loss of the summit seismic stations compromised AVO's ability to locate earthquakes during the latter portions of the eruption. The summit stations also provided the means with which to track the microseismicity occurring within the edifice, which was detectable only at those stations. Although not available in real time, the campaign broad-band data provided three-component records of high dynamic range with a flat response in the frequencies of interest. The 24-bit dynamic range allowed the entire eruption sequence to be recorded on scale.

The seismic data collected from the 2006 eruption of Augustine Volcano provide an excellent dataset for calibrating event classification schemes. A wide range of nonseismological observations complement this dataset, including deformation and visual records, as well as surface temperatures measured via satellite, all of which serve as independent verifications of volcanic processes observed in the seismic dataset. Perhaps most importantly, the eruption exhibited several types of activity, including a precursory earthquake swarm, vulcanian explosions, and sustained ash emission, in a 1-month time frame. This complexity provides the opportunity to benchmark tools against a variety of volcanic events in a single dataset.

Our analysis is based on a custom earthquake catalog. The analyst-reviewed earthquake catalog produced by AVO is limited to events that meet specific quality criteria (Dixon and others, 2008). For the current analysis we wished to include emergent earthquakes that cannot be located by traditional methods. We also wanted coverage of the final explosions and the transition into the continuous phase, even though the loss in summit stations compromised earthquake location during those periods. To accomplish this, we compiled a custom catalog of earthquakes for the period of time between January 1 and February 6. We scanned the full set of continuous waveforms and included in the catalog all earthquakes observed on a minimum of three stations including AU13, regardless of whether the trace was impulsive or emergent. Requiring a clear signal on station AU13 introduced a minor station bias in the data. In practice, however, there were few earthquakes visible away from the summit that were not well recorded on AU13. By requiring all arrivals to appear on one consistent station, we were able to catalog events by their arrival time at AU13 instead of the traditional method of cataloging events by their modeled origin time. This allowed us to analyze earthquakes that were not locatable, either because of poor station coverage or emergent onset. Of the 3,514 events in this catalog, 39 percent were included in the AVO analyst-reviewed catalog. This difference helped insulate the analysis from network changes and allowed a more comprehensive inclusion of earthquake types—at the notable expense of earthquake locations. We chose AU13 as our master station because it had the lowest signal-to-noise ratio of the campaign broadband stations and, unlike most of the telemetered stations located at similar distances, recorded continuously through the eruption. All broadband stations at Augustine were instrumented with Guralp CMG-6TD (30 s) seismometers recording at 100 Hz.

Teleseismic signals (including regional earthquakes) were identified by referring to mainland seismic stations OPT and MMN, situated at sufficiently great distances from Augustine Island so as not to record the volcanogenic signals, and were not included in the catalog.

## Frequency Index Analysis

### Method

The frequency content of an earthquake is a first-order metric with which to infer different source processes. The frequency with the greatest amplitude in the Fourier spectrum, the so-called dominant frequency, can be used as a general proxy for spectral content. Dominant frequency has been used in studies to characterize waveform types (for example, Latter, 1980; McNutt, 2002), but several shortcomings arise when using dominant frequency as a measure of the overall frequency content. Earthquakes with low signal-to-noise ratios are subject to low-frequency noise contamination (a particular issue for broadband data); the high-frequency earthquake shown in figure 2, for example, has a dominant frequency of 1.27 Hz, despite its considerable high-frequency content. The dominant frequency measure is also unable to identify earthquakes with bimodal frequency distributions, measuring only one peak in the spectra and therefore grouping it with other single-peaked events. This is a particular issue for hybrid-type earthquakes. Our early attempts to classify waveforms on the basis of dominant frequency were unsuccessful, in large part because hybrid events were arbitrarily grouped with either the high- or low-frequency groups, depending on which peak in the spectrum happened to be largest. These uncertainties associated with dominant frequency led us to seek a more robust metric for discriminating between different types of earthquake.

We develop the frequency index ( $FI$ ) based on the ratio of energy in low and high frequency windows. Because the resulting measure spans many orders of magnitude, we use a base-ten logarithm to reduce the index to a simple number, typically between  $-3$  and  $1$  for this dataset. The logarithm is intuitively appealing because waveforms with equal amounts of high and low energy (as defined by the frequency windows) have a frequency index of  $0$ . A negative  $FI$  means the waveform is dominated by low-frequency energy, while a positive  $FI$  demonstrates a majority of energy in the high-frequency band.

We define the frequency index as

$$FI = \log_{10} \left( \frac{\text{mean}(A_{\text{upper}})}{\text{mean}(A_{\text{lower}})} \right), \quad (1)$$

where  $A_{\text{upper}}$  are the spectral amplitudes across a band of high frequencies and  $A_{\text{lower}}$  are the spectral amplitudes measured

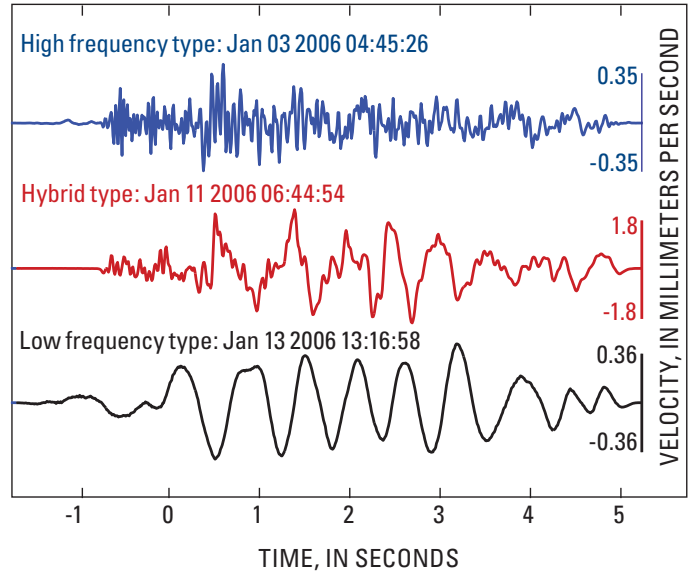


**Figure 2.** Selection of seismic waveforms from the “calibration set” used to translate between Frequency Index ( $FI$ ) and the high-frequency, hybrid, and low-frequency earthquake classification. Waveforms were selected on the basis of visual criteria.

across a lower range of frequencies. To calculate the  $FI$  in a consistent manner on thousands of waveforms, we use unfiltered waveforms with durations of 7 seconds: 1 second prior to the earthquake onset and 6 seconds after, ensuring that the high frequency P-wave onset is fully captured in the Fourier analysis. This is a sufficient time window over which to sample both the shorter duration, smaller magnitude earthquakes recorded, as well as the more emergent, lower frequency events. Linear trends and offsets are removed from the waveforms, and they are transformed to the frequency domain using a Tapered Fourier Transform. There is no need to correct for instrument response during this particular analysis, because the data were recorded on sensors with a flat response across our bandwidth of interest.

To determine suitable ranges for  $A_{\text{lower}}$  and  $A_{\text{upper}}$  we compiled a set of calibration waveforms. Using standard, if subjective, visual criteria, we selected high quality examples of three types of earthquake, based on the canonical high-frequency, low-frequency, and hybrid volcanic earthquake classification scheme (for example, Minikami, 1960; Lahr and others, 1994; McNutt, 1996). The high-frequency earthquakes contain energy up to 30 Hz; the low-frequency earthquakes contain a range of frequencies predominantly between 1 and 4 Hz; while the hybrid-type earthquakes sample both. Figure 2 shows example waveforms of high-frequency, hybrid and low-frequency type waveforms from this set. The frequency spectra for each event type were stacked to produce the spectra in figure 3A. The spectra were normalized to the area below each spectral curve prior



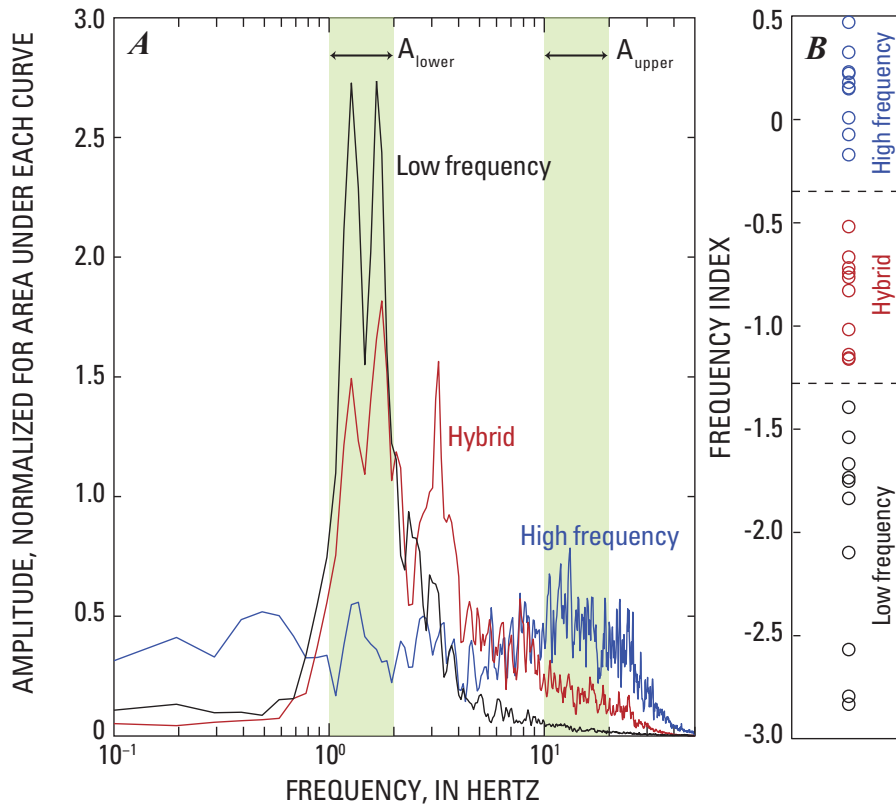


**Figure 3.** Frequency spectra and  $FI$  values for the “calibration set” of waveforms used to translate between Frequency Index ( $FI$ ) and the high-frequency, hybrid, and low-frequency earthquake classification. **A**, Stacked frequency spectra of 10 high frequency, 10 low frequency and 10 hybrid “calibration waveforms,” normalized for area beneath the curve. Ranges for  $A_{upper}$  and  $A_{lower}$  are displayed as shaded areas. **B**,  $FI$  values for each waveform, with dashed black lines indicating the half-distance between earthquake types.

to stacking. The intervals for  $A_{lower}$  and  $A_{upper}$  were defined across frequencies where the differences between the high-frequency, low-frequency and hybrid earthquake spectra were most pronounced:  $A_{lower}$  was attributed the range of 1-2 Hz, while  $A_{upper}$  was set to the range of 10-20 Hz, as shown in figure 3A. The  $FI$  values were calculated for the sample set and are shown in figure 3B. Although the frequency ranges in equation 1 are subjectively defined, the  $FI$  provides a repeatable quantitative measure of the frequency content inherent to the waveform. The calibration earthquakes provide an approximate translation between  $FI$  and the more traditional high-frequency, low-frequency, hybrid paradigm.

The high frequency, low frequency and hybrid groups fall within distinct  $FI$  limits, showing no overlap between groups, and exhibit an overall range of  $FI$  values between -2.9 and 0.5. Black dashed lines in figure 3B mark the half-distance between the group end-members at -0.4 for the transition from high frequency to hybrid earthquakes and at -1.3 for the transition from hybrid to low frequency earthquakes. The threshold for high frequency earthquakes is less than 0, which is not intuitive, since the 0  $FI$  represents equal amplitudes at high and low frequencies. Indeed, the overall distribution of  $FI$  is biased towards the lower frequencies. There are two causes for this. The first is the greater attenuation of high frequencies with distance from the earthquake source. The second is the generally low signal-to-noise ratio of the high frequency earthquakes. This is due to the small magnitude of the seismicity (the largest located earthquake

during the entire eruption had  $M_L$  1.5, Dixon and others, 2008) and high levels of low-frequency noise resulting from the location of Augustine Island. These two factors tend to amplify the low frequency end of the spectrum. An examination of larger magnitude high-frequency earthquakes in other settings suggests that  $FI$  values of 1 and 2 should be common outside of this particular dataset.

### **$FI$ Analysis for the Eruption Sequence**

The distribution of  $FI$  values shows a distinct pattern with the eruptive phase (fig. 4). Before the swarm on January 10–11, the majority of events had significant amounts of high frequency energy as indicated by the  $FI$  values greater than -0.5, with rare events as low as -1.8. The earthquakes during the preeruptive swarm were different, exhibiting  $FI$  values between 0.6 and -1.7, with 80 percent between 0.2 and -0.8. These ranges indicate that the earthquakes still contain significant amounts of high frequency energy, but that lower frequencies are present too; less than 10 percent of the earthquakes show dominantly low frequency (below  $FI$  -1.3) energy content. After the first two explosions on January 11, the earthquakes shift to a lower  $FI$ , between -0.2 and -1.2, indicating that they are predominantly hybrid-type earthquakes. In the 12 hours before the first magmatic explosion on January 13 (Wallace and others, this volume), the  $FI$  range drops further to  $FI$  s of -0.5 to -1.6. In the hour prior to the first of the explosions on January 13, the  $FI$  drops as low as -2.9. Throughout

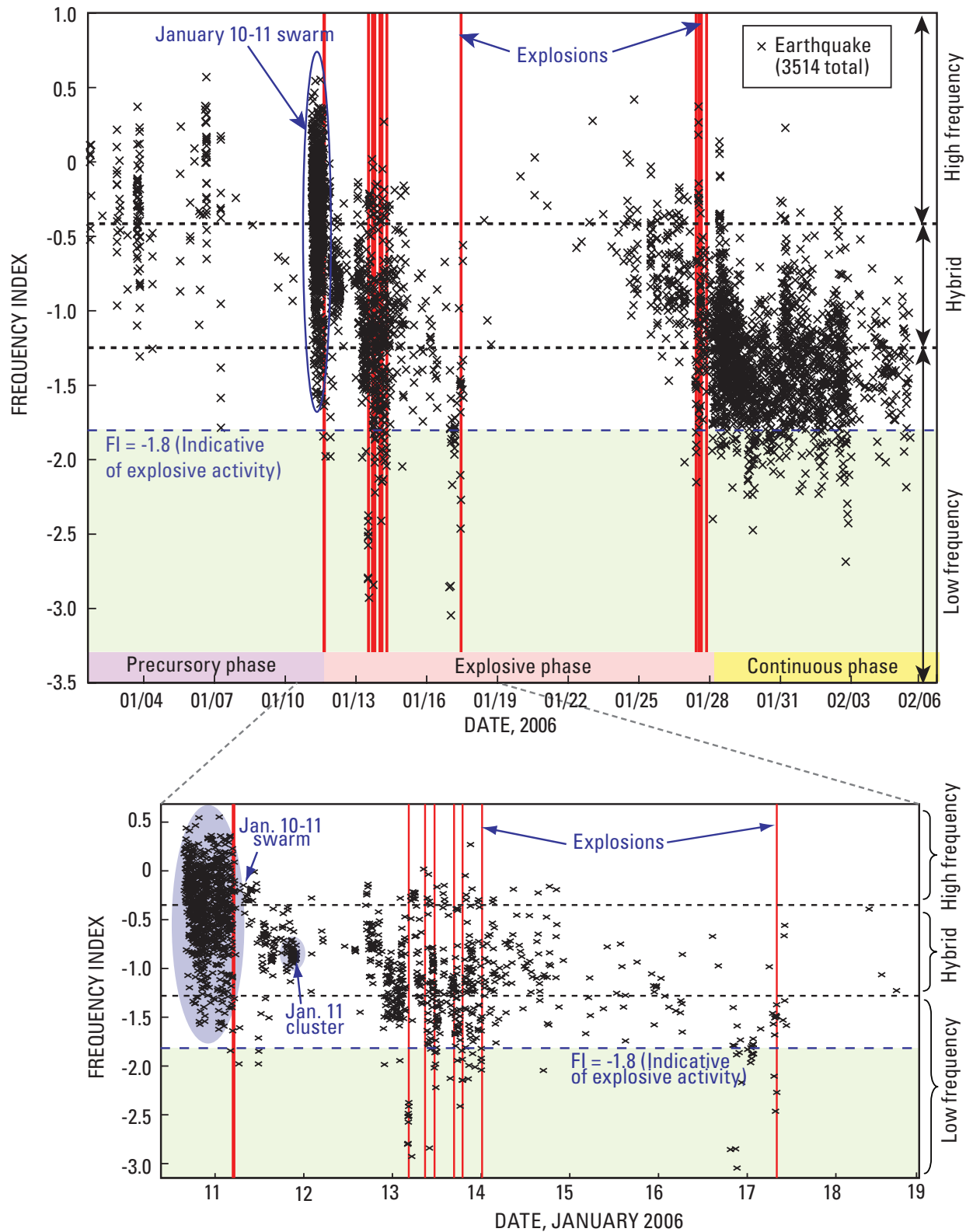


**Figure 4.** Distribution of Frequency Index ( $FI$ ) with time at station AU13 for all earthquakes in the custom Augustine earthquake catalog. The  $FI$  range for the Augustine dataset is between 0.57 and  $-3.05$ . Explosions are marked with vertical red lines.  $FI = -1.8$  (dashed line at the top of the shaded area) indicates the threshold  $FI$  for earthquakes as precursors to explosive eruptions. Translation to the traditional high-frequency, hybrid, and low-frequency classification scheme is marked by dashed black lines at  $FI = -0.35$  and  $FI = -1.28$ .

the six explosions on January 13–14 the  $FI$  ranges from 0 to  $-2.9$ , with the majority of events between  $-0.7$  and  $-2$ . Once the explosive activity ceases, the range diminishes somewhat, with most earthquakes falling within the  $FI$  range of  $-0.5$  and  $-1.8$ , indicating hybrid and low frequency earthquake activity. A drop in  $FI$  is observed in the 12 hours prior to the explosion on January 17, with values as low as  $-3$ . After this explosion the seismicity decreases, and few events occur between January 17 and 25. Seismic activity resumes after January 25, and there is a systematic decline in the  $FI$  from  $0.4$  and  $-2$  leading up to the magmatic explosions on January 27–28. Following the last of the 5 explosions on January 28, the  $FI$  remains low. The earthquake activity from January 28 through February 6 falls mostly between the  $FI$  values of  $-0.4$  and  $-2$ .

Path and site effects can cause the frequency content of waveforms to vary significantly between stations. To verify the trends observed within the  $FI$  results,  $FI$  analysis was carried out at station AU15 located 3.5 km southwest of the edifice (fig. 1). The  $FI$  for these earthquakes was calculated using the same procedure described for the AU13 arrivals, with results shown in figure 5. The  $FI$  trends observed at station AU15 are similar to those found at station AU13, showing the same high  $FI$  values prior to the eruption sequence and a significant drop after the precursory swarm. The same association between low  $FI$  events and explosions is observed at AU15. In general, however, the upper  $FI$  values at AU15 are lower than those at AU13. Another difference between the  $FI$  at these

stations is observed during the continuous phase. The majority of earthquakes at AU13 have  $FI$  values between  $-1$  and  $-2$ , whereas the majority of events at station AU15 fall between  $-0.5$  and  $-1.5$ , and the pronounced drop in  $FI$  seen at station AU13 after January 28 is scarcely evident at AU15. Strong wind can increase the  $FI$  of an earthquake, because it introduces high frequency noise into the spectrum and lowers the signal-to-noise ratio. It is possible that the poor weather conditions during the continuous phase had a greater effect on the signal-to-noise ratio at station AU15 than at AU13, given that the prevailing northwesterly wind direction affords minimal shelter to a site on the west of the island such as AU15. We consider wind noise to be one possibility for the  $0.5$   $FI$  variation between these two stations.

### Interpretation of Eruptive Sequence in Terms of $FI$

One of the most notable features of the eruption was the energetic swarm of earthquakes characterized by high  $FI$  values (up to  $0.5$ ) in the hours preceding the first explosive eruption on January 11. The predominance of high frequencies suggests that much of the energy was released by fracturing rock. We interpret this as the final opening of the conduit pathways to the surface, which facilitated the first of the explosions. The first two explosions were predominantly gaseous and contained little ash (Wallace and others, this volume),

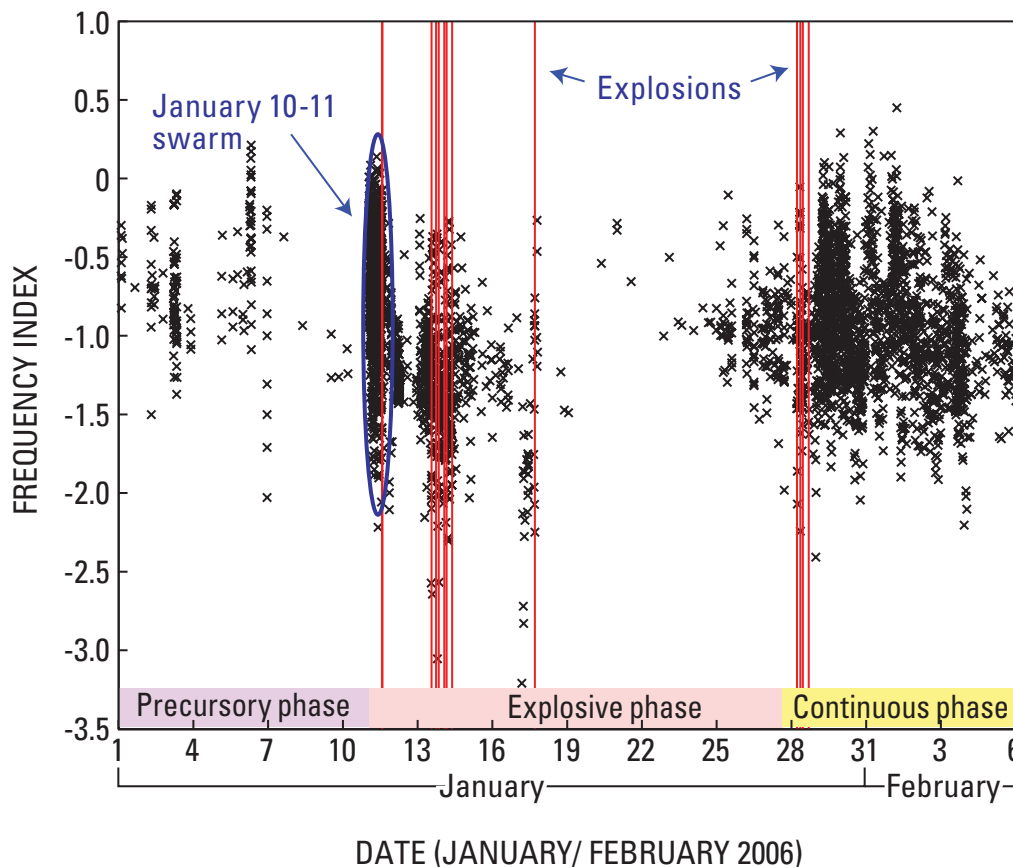


**Figure 5.** Frequency Index ( $FI$ ) for the catalog recorded at station AU15. Explosions are marked with vertical red lines.

**Table 1.** Summary of earthquake clusters and *FI* associated with volcanic explosions at Augustine Volcano, Alaska, January 11–28, 2006.[AKST, Alaska Standard Time; *FI*, Frequency Index]

| Day, 2006            | Time, AKST | Number of events in cluster prior to explosion | Length of cluster | Time between end of cluster and explosion | Maximum correlation within cluster | <i>FI</i> range of cluster | Number of events with <i>FI</i> < -1.8 since last explosion | Plume height, kilometers above sea level |
|----------------------|------------|--|-------------------|---|------------------------------------|----------------------------|---|--|
| Jan. 11              | 0444       | <swarm>  | -                 | 13 min                                    | -                                  |                            | 1   | 9  |
| Jan. 11 <sup>1</sup> | 0512       | 0  | -                 | -   | -                                  |                            | 0   | 9  |
| Jan. 13              | 0424       | 5  | 10 min            | 1 min                                     | 0.97                               | -2.35 -> -2.8              | 9   | 10                                       |
| Jan. 13              | 0647       | 9  | 56 min            | 1 hr 17 min                               | 0.96                               | -1.03 -> -1.3              | 2   | >9                                       |
| Jan. 13              | 1122       | 11   | 15 min            | 16 min                                    | 0.98                               | -0.93 -> -1.28             | 3   | 11                                       |
| Jan. 13              | 1640       | 5  | 17 min            | 13 min                                    | 0.92                               | -1.07 -> -1.28             | 6   | 10                                       |
| Jan. 13              | 1858       | 0  | -                 | -   | -                                  |                            | 6   | 9  |
| Jan. 14              | 0014       | 0  | -                 | -   |                                    |                            | 9   | no data                                  |
| Jan. 17              | 0758       | 6  | 37 min            | 6 hr 23 min                               | 0.91                               | -1.78 -> -1.92             | 15  | 14                                       |
| Jan. 27              | 2024       | 29   | 81 hr 13 min      | 9 hr 24 min                               | 0.95                               | -0.5 -> -1.5               | 1   | 9  |
| Jan. 27              | 2337       | 0  | -                 | -   | -                                  |                            | 4   | <3                                       |
| Jan. 28              | 0204       | 0  | -                 | -   | -                                  |                            | 0   | 8  |
| Jan. 28              | 0742       | 0  | -                 | -   | -                                  |                            | 0   | 8  |

<sup>1</sup> Disregarded because this explosion occurs within half an hour of the previous event.

suggesting that the high frequency fracturing preceding the eruption was driven by high-pressure gas moving ahead of the magma that followed in later eruptions. The precursory swarm on January 10–11 also contained a small number of events with *FI* as low as  $-1.6$ . These events are more consistent with a source generated from the migration of fluids. One possibility is that on January 10–11 magma within the Augustine edifice began to move slowly upwards. As the pressure on the magma decreased, additional water exsolved from the magma, creating a gas phase. This high-pressure gas phase migrated rapidly to the summit ahead of the magma, opening pathways and enabling magma to follow in the subsequent eruptive sequence.

These first two explosions were followed by a 2-day repose period, during which the average *FI* dropped to values between  $-0.2$  and  $-1.2$ , with a notable 2-hour-long cluster of repeating earthquakes all with *FI* values near  $-0.9$  (fig. 4). These hybrid and low frequency events were likely caused by the movements of magma into shallow levels of the edifice in anticipation of explosive eruption. The presence of hybrid earthquakes (*FI*  $-0.4$  to  $-1.3$ )—and therefore some amount of high frequency energy—suggests that pathways to the surface were still not entirely open and brittle fracture continued as magma continued to force open conduits and/or squeeze through constrictions. The net effect, however, was to bring magma into shallow levels in the volcano. Cervelli

and others (this volume) reach a similar conclusion, based on the deformation signals recorded at the summit, and suggest an upward propagating magma-filled crack near GPS station AV05 (fig. 1). Coombs and others (this volume) further propose that a small and relatively degassed lava dome effused on January 12, which was subsequently destroyed during the sequence of magmatic explosions on January 13–14.

### *FI* as an Eruptive Precursor

Earthquakes with *FI* values lower than  $-1.8$  are seen exclusively within 17 hours of the larger explosions in January 2006 and occur frequently during the continuous eruptive activity in late January and early February, diminishing in number with the gradual decline of explosive activity. Such a close association between explosions and low-*FI* earthquakes strongly suggests that these earthquakes are directly related to the explosive process. These results are summarized in table 1.

Low frequency earthquakes prior to eruption sequences are not unique to Augustine and have been observed in a variety of places, including Redoubt (for example, Chouet and others, 1994), Galeras (for example, Fischer and others, 1994), and Pinatubo (Harlow and others, 1994). The time scales over which these events occur vary between systems, ranging from hours to weeks, and are thought to depend on the amount



of pressurization within the magmatic/hydrothermal system below the volcano (Chouet, 1996). The time scale of 17 hours at Augustine Volcano is similar to the build-up observed before the December 1989 eruption of Redoubt and is consistent with a system which has become pressurized.

The occurrence of low- $FI$  earthquakes prior to explosive eruptions suggests that they are linked to the movement of magmatic fluids preceding extrusion. This is a significant observation from a monitoring perspective, as it presents a tool with which explosive eruption events might be anticipated. An empirical threshold of  $FI < -1.8$  for this dataset, as indicated on figure 4, successfully anticipates explosive events or sequences. One earthquake with an  $FI$  of  $-2.1$  occurred late on January 14, 17 hours after the final explosion of the January 13–14 eruptive sequence and did not occur as an explosion precursor. However its occurrence so soon after the powerful January 13–14 explosion sequence could mean that it was the final low- $FI$  event from that sequence. Regardless, it is clear from table 1 that the limit of  $-1.8$  never failed to indicate a pending explosion series, being successful for 10 of the 13 individual large explosions.

## The Role of Attenuation

Because the  $FI$  analysis is based on waveform amplitude in different frequency bands, it will be influenced by attenuation effects. Seismic waves are diminished as a function of distance and frequency by a combination of intrinsic attenuation and scattering attenuation. The attenuating character of the Earth can be expressed through the quality factor  $Q$ , which is related to the seismic amplitude by

$$A(\omega, r) = A_0 r^{-n} \exp(-\omega r / 2Qv), \quad (2)$$

where  $A(\omega, r)$  is the spectral amplitude as a function of angular frequency  $\omega$  and distance  $r$  from the source (Aki and Richards, 1980).  $A_0$  is the amplitude at the source,  $v$  is the propagation velocity, and  $r^{-n}$  is the geometric spreading factor, where  $n=1$  for body waves and  $n=1/2$  for surface waves. To determine the influence of attenuation on  $FI$ , we combine equations 1 and 2. We simplify the system by approximating the lower and upper frequency ranges by their center (angular) frequencies,  $\omega_{upper}$  and  $\omega_{lower}$ :

$$FI(Q, r) = \log_{10} \left[ \frac{A_{upper0} r^{-n} \exp(-\omega_{upper} r / 2Qv)}{A_{lower0} r^{-n} \exp(-\omega_{lower} r / 2Qv)} \right], \quad (3)$$

$$FI(Q, r) = \log_{10} \left[ \exp \left( -\frac{r}{2Qv} (\omega_{upper} - \omega_{lower}) \right) \right] + \log_{10} \left[ \frac{A_{upper0}}{A_{lower0}} \right], \quad (4)$$

$$FI(Q, r) = \log_{10} \left[ \exp \left( -\frac{r}{2Qv} (\omega_{upper} - \omega_{lower}) \right) \right] + FI_0, \quad (5)$$

where  $FI_0$  is the  $FI$  at the source. The form of equation 5 is significant because it demonstrates that attenuation will reduce  $FI$  by a fixed term but will not change trends in the  $FI$  data coming from a single source region. In other words, if one is willing to assume an attenuation and velocity,  $FI$  can be corrected for distance by a static correction term. This result is shown in figure 6, where we consider the case when  $FI$  is 0 and vary the distance for different values of  $Q$ .  $FI$  decreases linearly with distance, and the effect is increasingly more pronounced at low  $Q$  values. In fact, this relation can be used in reverse to estimate attenuation directly using  $FI$  measured at a range of epicentral distances.

The above analysis makes several assumptions. We do not take into account the differential effect of attenuation within the frequency ranges specified by  $A_{upper}$  and  $A_{lower}$ . Since our frequency ranges are narrow, we approximate attenuation effects at the center frequencies across  $A_{upper}$  and  $A_{lower}$ , 15 and 1.5 Hz, respectively. The error introduced by this assumption is smaller than the variations introduced by an assumed  $Q$  value. We also assume a constant value of  $Q$ , contrary to the findings of studies of attenuation in other volcanic areas (such as Patanè and others, 1994), where  $Q$  is found to vary across orders of magnitude within single volcanic complexes.

## Shortcomings of the $FI$ Method

The Frequency Index technique worked well for the Augustine 2006 eruption, showing trends in seismicity that were otherwise difficult to quantify. Its success is largely due to the high-quality, close range dataset. The method would

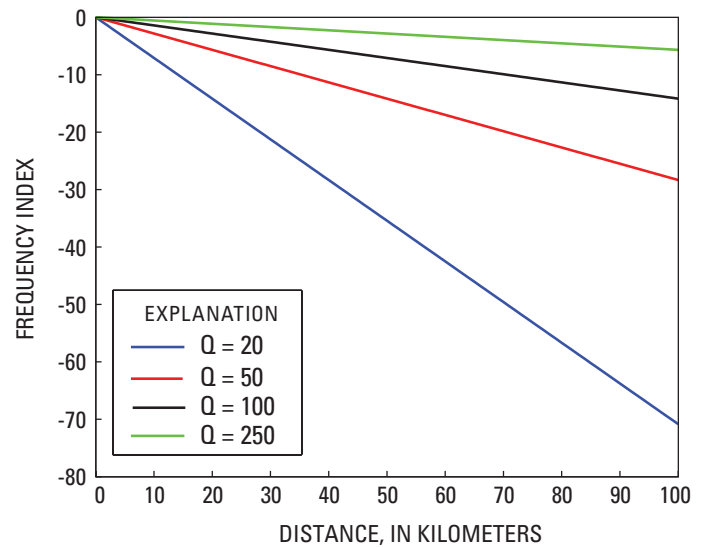


**Figure 6.** Frequency Index plotted against distance for different (fixed) values of the quality factor  $Q$ . The subsurface velocity was set to 1.3 km/s.

have been less successful at stations with poorer signal-to-noise ratios. The low-frequency bias evident in the model waveform set reflects this problem and indicates a fundamental challenge to quantifying the frequency content of small-amplitude seismic signals. It is possible that other datasets will be less contaminated by low-frequency noise than this dataset because the location of Augustine Island and the North Pacific wintertime storm conditions that prevailed during much of the eruption make for a seismically noisy environment. It is clear that site effects must be carefully considered when evaluating trends in *FI*, because they introduce an inherent bias within the *FI* calculation. This is demonstrated through the differences between figures 4 and 5 where station AU15, located in a particularly windy area of the island, yields much noisier data and lower values of *FI*.

Volcanic tremor could also influence the *FI* analysis. Our interval for  $A_{\text{lower}}$  (1–2 Hz) is within the common frequency range for volcanic tremor (for example, Gordeev, 1992), and it is possible that background tremor could add a low-frequency bias to the *FI*. Although potentially detrimental to the *FI* analysis, this may prove to be useful from a monitoring perspective. Volcanic tremor is often (although not always) associated with volcanic eruptions (Chouet, 1981), and an earthquake with a low *FI* due to tremor is also likely to be associated with a volcanic eruption. It therefore does not necessarily detract from the association between low *FI* and imminent eruption.

## Repeating Earthquakes

Waveform similarity is another method for investigating trends in earthquake activity within large datasets. Recurring waveforms are significant because they are the product of earthquakes occurring in nearly the same place with the same mechanism. Not only do repeating events reveal the characteristic time of the seismogenic source, they can also be exploited for high-resolution mapping of the source volume. Stephens and Chouet (2001) and Green and Neuberg (2006) have used repeating low-frequency earthquakes to demonstrate that the sources of some low-frequency events are long lived, despite changes in a volcano's eruptive state. These events have been attributed to recurring interactions between magma and a fixed conduit geometry. Recurring high-frequency waveforms have been exploited by several authors to obtain precise relative relocations that define the timing and spatial extent of dike and fault structures within a volcanic edifice (for example, Got and others, 1994; Rowe and others, 2004; Thelen and others, 2008; DeShon and others, this volume). Here we explore the role of repeating earthquakes as precursors to explosive eruptions.

## Method

We use cross-correlation to measure the similarity of waveforms in the event catalogue discussed above, again using station AU13. Focusing on a single station precludes

the use of location techniques (see DeShon and others, this volume) but allows us to work with a more comprehensive catalog, improving time resolution and allowing us to extend the analysis into the latter portions of the eruption when all of the summit stations had been destroyed. Except for a handful of earthquakes at depths between 3.5 and 4.5 km, the located earthquakes all emanate from a relatively tight source region (Dixon and others, 2008; Power and Lalla, this volume), suggesting that the same is true for our more extensive catalog.

To calculate waveform cross-correlation, we extract a 6-second window of vertical component data beginning at the picked arrival time. Six seconds of data following the pick is sufficient to capture the largest amplitude sections of most waveforms (which dominate the cross-correlation) while minimizing the influence of background noise on short high-frequency waveforms. Changes in the window length of a few seconds showed only a minor influence on the correlation coefficients (not shown).

Each waveform in the dataset is correlated against all other waveforms using an algorithm tailored to large datasets using the newly developed waveform correlation toolbox for MATLAB (<http://www.giseis.alaska.edu/Seis/EQ/tools/GISMO>, accessed September 7, 2009). In the first step, all waveforms are transformed into the frequency domain. The first frequency-domain waveform is then multiplied against every other waveform, equivalent to convolution in the time domain. Exploiting the symmetry of the problem, the second waveform need only be multiplied by the third and subsequent waveforms, and so forth. This is equivalent to filling in the upper matrix triangle in figure 7 and completing the rest through a symmetry argument. The resulting cross-correlation series are transformed back to the time domain, where second-order polynomial interpolation is used to estimate the sub-sample maximum cross-correlation value. The maximum of the cross-correlation is normalized, following convention, to the scale of –1 to 1. The maximum value and its associated lag time are saved into  $n$  by  $n$  matrices, where  $n$  is the number of traces. Hereafter we refer to the normalized maximum of the cross-correlation function as simply the correlation value. The lag values are used to align the traces in time.

Figure 7 shows the similarity matrix for all events, chronologically left to right and top to bottom (not evenly spaced in time), with one pixel for each pair of waveforms. The matrix is symmetric with unity on the diagonal. Although figure 7 hardly does justice to the 10 million correlation values that form the matrix, it is clear that the majority of earthquakes throughout the eruption show little similarity. (Because we search for the optimum correlation lag times, even unrelated waveforms will often correlate at 0.5 or better.) Within this dataset, however, there are numerous clusters and time patterns with direct implications for volcanic processes (Buurman and West, 2006). The challenge is to mine the dataset in intuitive ways. We identify clusters using a hierarchical clustering method similar to that used by Rowe and others (2002). First we link all events on the basis of their correlations (fig. 8). Branches within the hierarchy are joined

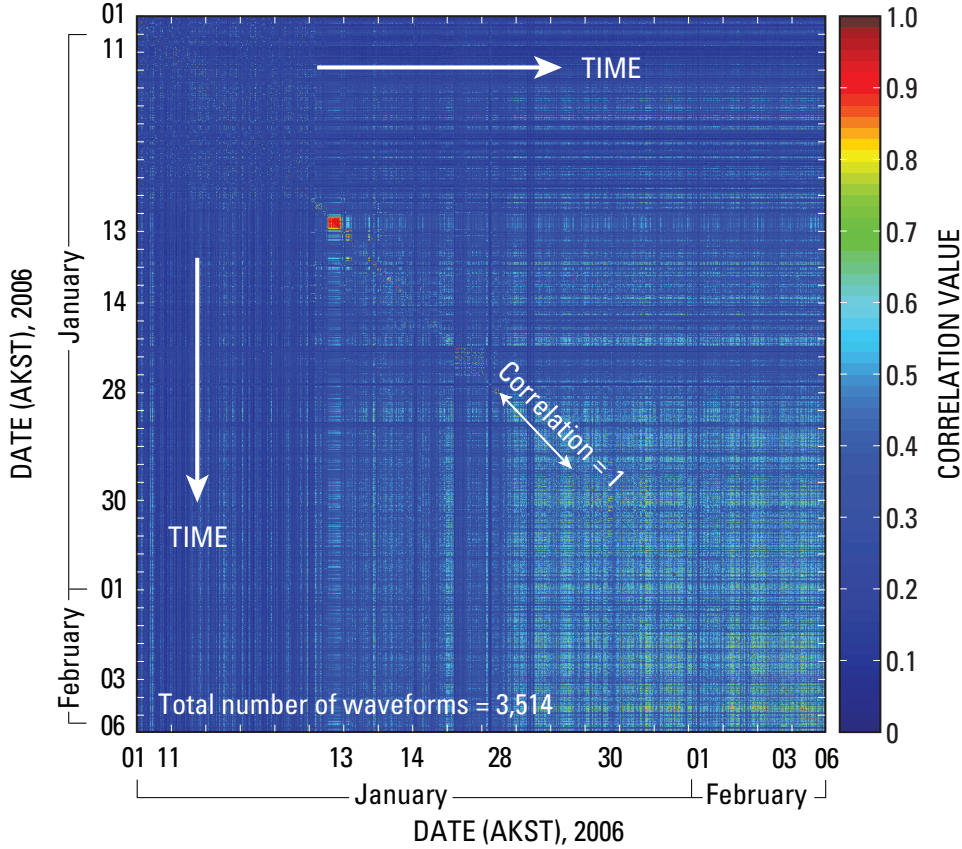


**Figure 7.** Correlation matrix for the entire Augustine 2006 catalog. Each point represents an earthquake correlation pair. The matrix is symmetric, with time progressing left to right and top to bottom. The correlations on the diagonal are equal to one as each waveform is auto correlated, although they appear muted because of the size of the matrix. The majority of cross-correlations in the dataset are poor, with values less than 0.6.

at nodes whose height is the mean correlation value between each pair of events spanning the two groups. That is,

$$C_{p,q} = \frac{1}{n_p n_q} \sum_{i=1}^{n_p} \sum_{j=1}^{n_q} C_{pi,qj}, \quad (6)$$

where  $C_{p,q}$  is the mean correlation between the  $n$ th events in groups  $p$  and  $q$ . These links may be between individual events or between clusters of events, depending solely on which linkage has the highest mean correlation. The formation of discrete clusters is then just a matter of selecting branches from the hierarchical cluster tree. Because the correlation value is influenced by the trace length, filter parameters, and frequency content of the waveforms, the choice of correlation threshold is somewhat arbitrary. Given the wide variety of earthquake types in our catalog, we choose a threshold of 0.8 based on visual inspection to define clusters in lieu of a more adaptive approach, such as that of Rowe and others (2002). The value 0.8 is on par with or somewhat higher than in comparable studies (Petersen, 2007; Green and Neuberg, 2006; Stephens and Chouet, 2001).

We refer to groups of similar waveforms as clusters. “Multiplet” and “clones” (for example, Frémont and Malone, 1987; Geller and Mueller, 1980; Thelen and others, 2008) are comparable terms. We prefer the term cluster because of the implied spatial proximity and avoid the term “swarm” because it suggests a similarity in time. We use cluster to indicate a

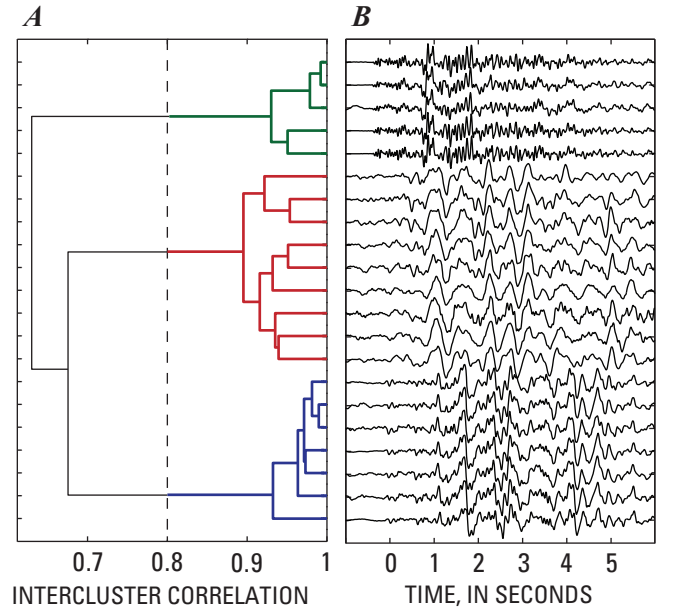


**Figure 8.** Illustration of the hierarchical clustering method used to group sample waveforms. *A*, The two most similar events are joined at a node, which yields a new correlation value. This value is then used to search the catalog for the next most similar event, pair, or group of events. Individual clusters are defined by assigning a minimum intercluster correlation value, indicated by the dashed line at 0.8. *B*, Waveforms corresponding to correlations in *A*.



similarity in waveform and, by extension, source location and mechanism. If a cluster occurs in a short period, it may also be a swarm, although this is not always the case.

In subsequent analyses we use a subset of data that includes the 40 largest clusters. This includes clusters of four or more events. By culling unrelated traces, trends not observed in figure 7 emerge as clear patterns that can be tied directly to different stages within the eruption (fig. 9A).

## Clusters of Similar Events Before Explosive Eruptions

The most important pattern in the subset matrix is the presence of repeating events in the hours preceding explosive eruptions. More than half of the ash-producing explosions during the explosive phase were immediately preceded by small clusters of highly similar earthquakes (“precursory clusters”). The two phreatic explosions at the beginning of the explosive phase were closely spaced in time and occurred at the end of the seismic swarm, which itself contained several clusters of earthquakes, discussed later. The first four explosions in the sequence of six ash-producing events on January 13–14 were preceded by small clusters (5–11 events) of similar earthquakes. These clusters occurred in short periods of time, some lasting only 10 minutes (table 1), and all occurred within 2.5 hours of eruption. The explosion on January 17 was preceded by a cluster that occurred 7 hours prior to eruption. The last four eruptions of the explosive phase, which occur immediately prior to the transition to continuous activity, show different seismic precursors than the other large explosions; they are preceded by an 81-hour swarm of earthquakes, not all of which are as strikingly similar as the previous precursory clusters. These results are summarized in table 1.

The largest cluster occurred on January 11 within the space of 2 hours and contained 57 events with exceedingly high correlation values (fig. 9D). This cluster was followed by a smaller but more protracted cluster that ended only 14 minutes before the first of the ash-producing explosions of the explosive phase. Earthquakes in the second cluster also showed similarity (values greater than 0.7) with the largest cluster, suggesting that the two clusters were slight variations of the same mechanism.

The occurrence of repeating clusters immediately prior to explosions indicates that they represent either the mobilization of magma, the opening of conduits to the surface, or both. The interaction of magma with surrounding rock is well known to produce repeating events. This association is most convincing during periods of dome growth, when magma extrusion is observed at the surface accompanied by repeating event clusters (for example, Thelen and others, 2008; Green and Neuberg, 2006). The same patterns were observed during the March 2006 lava effusion at Augustine (not shown). Conduit opening prior to explosive eruptions

is another viable option for the source of event clusters. In order for magma to erupt explosively, an open conduit to the surface is required. The magma ascent and gas exsolution that precedes explosions may well be responsible for creating (or reopening) such pathways to the surface (fig. 10). The progressive fracturing of a crack pathway, driven by high-pressure gas or fluid, is thought to be a mechanism for earthquake swarms (for example, Hill, 1977) and could produce nearly the same waveform. Although cracking is an inherently destructive process, a series of small progressive fractures on the same pathway would have the same mechanism and nearly the same seismic raypath. This would be an unlikely mechanism to explain many thousands of repeating events (for example, Petersen, 2007), but it is a more reasonable mechanism at Augustine, considering the modest size of the clusters preceding explosive eruptions.

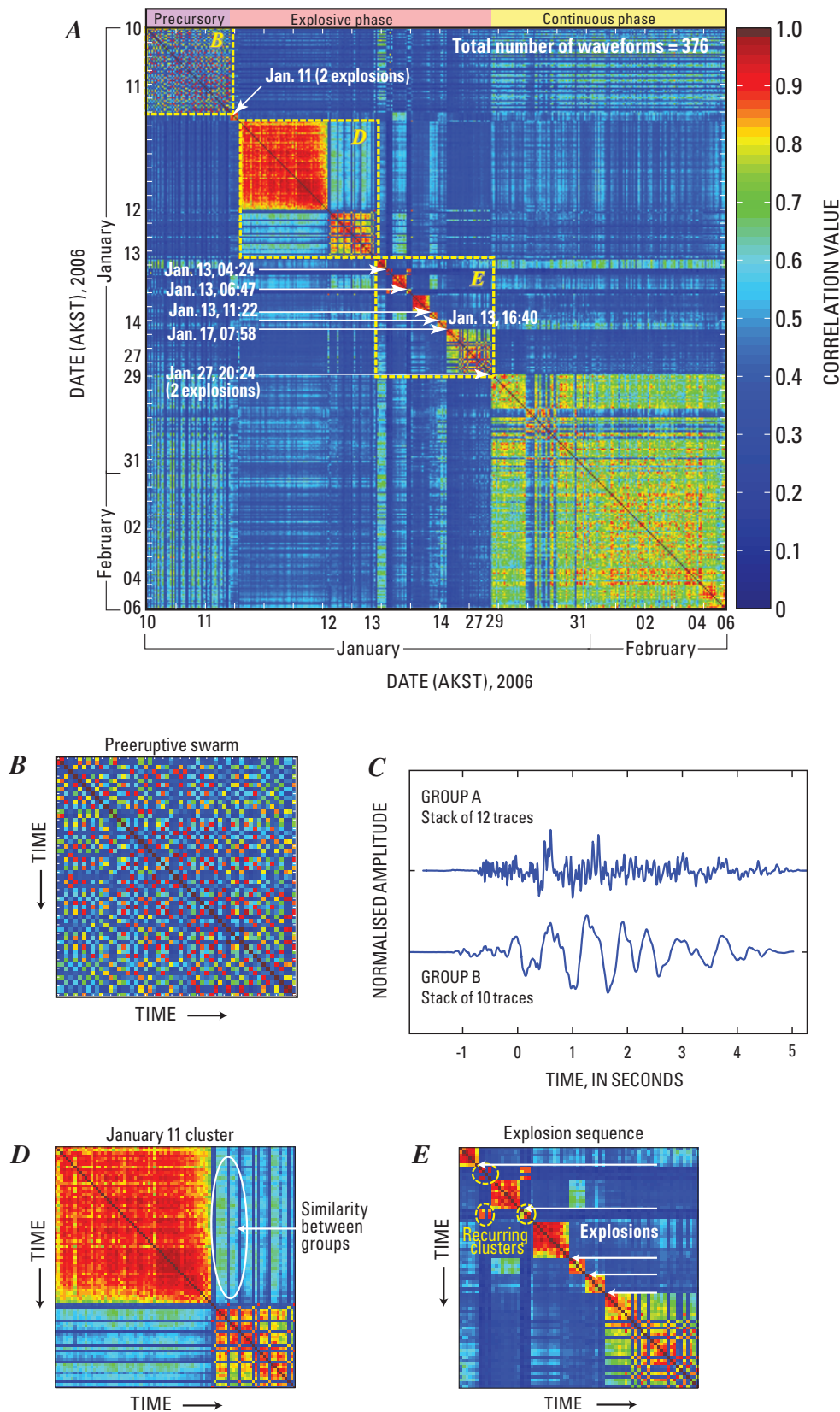
## Recurring Clusters

Figure 9A reveals a few occasions when a cluster of events pauses and resumes at a later time. A striking example of recurring clusters occurs on January 13 (fig. 9E). Two clustered swarms are separated by a gap of 3 hours but have events correlating as high as 0.9. This is seen by the high off-diagonal correlation values between the two swarms. These two small clusters occur immediately after explosions, suggesting that they are caused by posteruptive processes related to relaxation of eruptive stresses in the edifice. Alternatively, they may be related to a final release of gas or magma from the explosion.

## Contemporaneous Groups of Repeating Events

Some clusters occur contemporaneously with other unrelated clusters. The repeating events in the preeruptive swarm on January 11 provide a good example. Within this group there are two main families of waveforms, referred to here as *A* and *B* (fig. 9C). The waveforms in group *A* contain significant amounts of high-frequency energy, indicated by their range in *FI* of  $-0.2$  to  $-1.4$ . Waveforms in the *B* cluster have lower frequency content ( $FI < -2.5$  for nine of the waveforms, with one outlier), although they also contain some portion of high-frequency content. Because both families occur during the same time period, the similarity matrix shows deceiving scatter when sorted chronologically (fig. 9B). The presence of two families, one rich in high frequencies, the other rich in low frequencies, demonstrates the coexistence of different seismic processes. Considering the vigor of this preeruptive swarm and its occurrence prior to the first explosive eruption, cluster *A* likely represents the brittle failure of rock caused by the incremental opening of cracks as a result of a new intrusion of fluids or gases in the shallow edifice. We attribute cluster *B*, rich in low-frequency energy, to resonances caused by this same movement of gas or fluid to shallow depths.





**Figure 9.** Refined correlation matrix (A), with sample waveforms (C), and enlarged sections of the matrix (B, D, E). A, Refined correlation matrix showing the 40 largest clusters. Explosions are marked with white arrows. Dashed yellow lines indicate enlarged areas (panels B, D, and E). B, Enlargement of the preeruptive swarm time period, showing disparate clusters of repeating events. C, Stacks of the two largest groups of waveforms present during the preeruptive swarm shown in B. D, Enlargement of the large clusters on January 11, containing correlation values as high as 0.97. E, Enlargement of the explosive phase, with recurring clusters circled. Explosions are marked with arrows.

## Repeating Earthquakes During Continuous Eruptive Activity

The character of the repeating earthquakes changes with the transition to the continuously explosive phase on January 28, 2006. Whereas the earlier explosive phase was characterized by intermittent swarms of highly clustered events lasting minutes to hours, repeating events during the continuous phase are more variable but seem to follow one general waveform type. Our arbitrary correlation criterion of 0.8 groups these events into several small clusters. However, the subset similarity matrix (fig. 9A) suggests that there is one dominant cluster beginning on January 28 that extends beyond the end of our analysis on February 6 as seismicity began to taper significantly. This cluster is interspersed by a smaller cluster of 21 events on January 29 and 30.

Poor weather during much of the continuous phase prevented visual and satellite-based observations for all but the largest explosive events. The emergent broad-spectrum seismic data was at times enigmatic. In the absence of corroborating evidence it was challenging to separate how much of the seismicity represented rockfall activity on the new dome and how much was generated by the emplacement of new lava at the surface. Although both sources were surely present, the retrospective similarity analysis demonstrates that a subset of the events can be tied directly to magma extrusion. Rockfall events, including pyroclastic flows and avalanches, are inherently dissimilar because of their chaotic and destructive mechanism. The repeating sequence could be stick-slip behavior associated with dome growth, as has been documented in the 2004 Mount St. Helens sequence (Moran and others, 2008). However, the low frequency nature (fig. 4) of the events, combined with their registration at all on-island stations and on the pressure sensor at AUE (not shown), suggest that vulcanian explosions are a more plausible source. Indeed, as the number of explosions declined during early February (evident on the pressure sensor at AUE, not shown), so too did the number of repeating earthquakes.

## Discussion

### Combining *FI* Data and Correlation Data

In order to gain further insight into the seismic activity using the similarity matrix in figure 9A it is helpful to compare these results with the *FI* analysis. Table 1 presents the *FI* values of the clusters that occurred prior to explosions (“precursory clusters”), as well as listing the number of earthquakes with *FI* below  $-1.8$  that occurred prior to each of the large explosion events. It is interesting to note that the very low *FI* earthquakes do not appear to occur in large clusters. Although events with *FI* below  $-1.8$  show a unique correspondence to explosive eruptions (see section on “*FI* as an eruptive precursor”), they are a separate phenomenon from the repeating

earthquakes. This suggests that they should be tracked independently and even that small numbers of very low *FI* events may have significant implications.

Not all explosions were preceded by precursory clusters or very low *FI* earthquakes. Almost all were preceded by one of the two, however. We disregard the second explosion of the sequence (table 1) because it occurs less than half an hour after the first. It is significant that 10 of the first 11 eruptions during the explosive phase were preceded by either repeating earthquakes or those with very low *FI*. Neither technique exhibits a significant change preceding the final two magmatic explosions of the explosive phase, which occurred immediately prior to the change to sustained eruptive activity. We suspect that by the time these explosions occurred, the volcano had already established a clear open conduit to the surface that allowed magma and gas to reach the surface without the constrictions present in early explosions. This suggests that both the frequency-based and correlation-based techniques (and likely all precursory seismic techniques) may perform better with initial eruptive activity than with ongoing repeat eruptions.

We hypothesize that both precursory clusters and very low *FI* earthquakes are associated with the movement of magma or, in some cases, gas. Specifically, we propose that the low frequency earthquakes are the result of the movement of magmatic fluids rising from the magma chamber (as proposed by Chouet, 1996), while the precursory hybrid clusters originate from the interaction between the advancing body of magmatic fluids and the brittle edifice (figure 10).

Although low frequency earthquakes and repeating earthquakes are commonly observed at volcanoes without eruption, the Augustine sequence provides unmistakable ground truth for these associations. By combining the two techniques, we see that although very low *FI* earthquakes can occur as precursory clusters, it is not generally the case and the two styles usually represent separate earthquakes.

## Adaptations for Real-Time Use

The *FI* technique shows promise as an indicator of explosive magmatic eruptions. It is also a useful all-purpose tool for quantifying trends in seismicity. *FI* is particularly useful in tracking changes in large numbers of earthquakes where manual inspection of waveforms is quickly overwhelmed. Examples include the transition from explosive to continuous activity at Augustine, or the changes from high-frequency to hybrid and lower frequency events observed during the early stages of the 2004–8 Mount St. Helens dome building eruption (Moran and others, 2008). It provides a repeatable, quantifiable measure that is simple to calculate and faithfully reduces the overall frequency content of a waveform to a single parameter.

The correlation approach is similarly well suited to large datasets where the pattern matching required to identify repeating clusters of events is all but impossible without

computational aids. Figure 7 provides an excellent example of how these rich correlation patterns in the Augustine sequence can be buried by high rates of scattered seismicity.

Both tools are readily adaptable to real-time use, and both techniques operate on short waveform segments encompassing a detected event but do not require event locations. This distinction is significant. A seismic event detection system is one of the most basic monitoring tools available at nearly all monitored volcanoes. Fully automated event locations, though existent, are still the exception at most volcanoes.

The *FI* parameter can be used in real time in its current form. All that is required is a real-time module to perform the trivial Fourier transform and ratio calculation and a database to store and track the progression of these values.

The correlation tool needs to be adapted slightly. In the analysis presented here, the complete seismic history of the eruption was already available, so that for a given moment in the eruption all events from the past and future could be used in the correlation. As a real-time tool, the correlation analysis must be limited to events that have already occurred. The easiest implementation would store the waveforms from detected events (or preferably store pointers to these waveforms in a continuous waveform archive). When a new event is detected, it

would be correlated against other events in the recent past. This could include all events in a fixed time frame (say, 12 hours), or it may be more computationally appropriate to include a fixed number of events (say, the past 100 detected waveforms). The only significant challenge in implementing a real-time correlation tool is computational expense, although this could be minimized by storing the most recent waveforms in memory. Storing the Fast Fourier Transform of each waveform would be even more efficient. By correlating each incoming event against recent waveforms instead of the entire dataset, the resulting similarity matrix would be limited to a strip of data within  $n$  steps of the diagonal, where  $n$  is the number of recent events included in the correlation calculation. In many cases this may be sufficient to reveal the basic similarity patterns, as demonstrated by Umakoshi and others (2008). In the Augustine 2006 dataset, for example, most correlation patterns are fully revealed when only the previous 150 events are included.

Both tools are simplistic in that they operate on single channels of data, though more comprehensive multichannel versions can be envisioned. The single-channel requirement makes them straightforward to implement, however, and given this simplicity we believe the frequency index and correlation tools can be readily incorporated into most processing systems. Although both tools have limitations and will not always be as insightful as they have proven for the Augustine 2006 eruption, we believe that they have the potential to become indispensable additions to the suite of seismic volcano monitoring tools.

## Acknowledgments

We thank Stephanie Prejean and Rick Aster for their helpful comments and suggestions. We also thank John Power, Kate Bull, and Katie Jacobs for several useful discussions that also improved the manuscript.

## References Cited

- Aki, K., and Richards, P.G., 1980, *Quantitative seismology*: New York, W.H. Freeman, 700 p.
- Bailey, J.E., Dean, K.G., Dehn, J., and Webley, P.W., 2010, Integrated satellite observations of the 2006 eruption of Augustine Volcano, in Power, J.A., Coombs, M.L., and Freymueller, J.T., eds., *The 2006 eruption of Augustine Volcano, Alaska*: U.S. Geological Survey Professional Paper 1769 (this volume).
- Benoit, J.P., and McNutt, S.R., 1996, Global volcanic earthquake swarm database, 1979–1989: U.S. Geological Survey Open-File Report 96-0069, 333 p.
- Buurman, H., and West, M., 2006, Integrated seismic observations of the 2006 eruption of Augustine Volcano: *Eos*

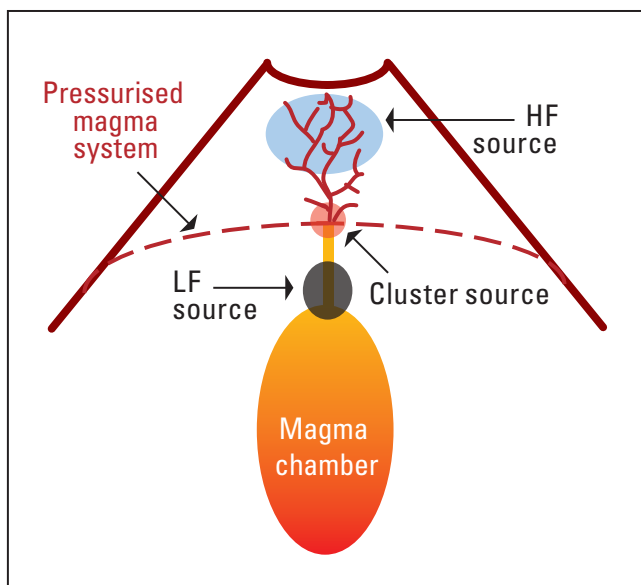


**Figure 10.** Schematic model showing the origins of high-frequency (HF) earthquakes, low-frequency (LF) earthquakes, and the (hybrid) clusters. Low-frequency earthquakes are generated by the movement of magmatic fluids, as proposed by Chouet (1996). Earthquake clusters have a tight source region, where both brittle fracture and fluid resonance occurs, at the head of the advancing body of magma. High-frequency earthquakes, such as those in the precursory swarm, are the result of the brittle fracture of rock in the edifice, where volatiles from the degassing body of magma break new pathways to the surface.



- (American Geophysical Union Transactions), v. 87(52), Fall Meeting supp., abs V51C-1683
- Cervelli, P.F., Fournier, T.J., Freymueller, J.T., Power, J.A., Lisowski, M., and Pauk, B.A., 2010, Geodetic constraints on magma movement and withdrawal during the 2006 eruption of Augustine Volcano, *in* Power, J.A., Coombs, M.L., and Freymueller, J.T., eds., The 2006 eruption of Augustine Volcano, Alaska: U.S. Geological Survey Professional Paper 1769 (this volume).
- Chouet, B.A., 1981, Ground motion in the near field of a fluid-driven crack and its interpretation in the study of shallow volcanic tremor: *Journal of Geophysical Research*, v. 86, no. B7, p. 5985–6016.
- Chouet, B.A., 1988, Resonance of a fluid-driven crack; radiation properties and implications for the source of long-period events and harmonic tremor: *Journal of Geophysical Research*, v. 93, p. 4375–4400.
- Chouet, B.A., 1996, Long-period volcano seismicity: its source and use in eruption forecasting: *Nature*, v. 380, p. 309–316.
- Chouet, B.A., Page, R.A., Stephens, C.D., Lahr, J.C. and Power, J.A., 1994, Precursory swarms of long-period events at Redoubt Volcano (1989–1990), Alaska—their origin and use as a forecasting tool: *Journal of Volcanology and Geothermal Research*, v. 62, p. 95–135.
- Coombs, M.L., Bull, K.F., Vallance, J.W., Schneider, D.J., Thoms, E.E., Wessels, R.L., and McGimsey, R.G., 2010, Timing, distribution, and volume of proximal products of the 2006 eruption of Augustine Volcano, *in* Power, J.A., Coombs, M.L., and Freymueller, J.T., eds., The 2006 eruption of Augustine Volcano, Alaska: U.S. Geological Survey Professional Paper 1769 (this volume).
- DeShon, H.R., Thurber, C.H., and Power, J.A., 2010, Earthquake waveform similarity and evolution at Augustine Volcano from 1993 to 2006, *in* Power, J.A., Coombs, M.L., and Freymueller, J.T., eds., The 2006 eruption of Augustine Volcano, Alaska: U.S. Geological Survey Professional Paper 1769 (this volume).
- Dixon, J.P., Stihler, S.D., Power, J.A., and Searcy, C., 2008, Catalog of earthquake hypocenters at Alaskan volcanoes; January 1 through December 31, 2006: U.S. Geological Survey Data Series 326, 79 p. [<http://pubs.usgs.gov/ds/326>, accessed September 7, 2009].
- Fischer, T.P., Morrissey, M.M., Calvache, M.L., Gomez, D., Torres, R., Stix, J., and Williams, S.N., 1994, Correlations between SO<sub>2</sub> flux and long-period seismicity at Galeras volcano: *Nature*, v. 368, p. 135–137.
- Frémont, M.J., and Malone, S.D., 1987, High precision relative locations of earthquakes at Mount St. Helens, Washington: *Journal of Geophysical Research*, v. 92, p. 10223–10236.
- Geller, R.J., and Mueller, C.S., 1980, Four similar earthquakes in central California: *Geophysical Research Letters*, v. 7, p. 821–824.
- Gordeev, E.I., 1992, Modeling of volcanic tremor wavefields: *Journal of Volcanology and Geothermal Research*, v. 51, p. 145–160.
- Got, J.-L., Frechet, J., and Klein, F.W., 1994, Deep fault plane geometry inferred from multiplet relative relocation beneath the south flank of Kilauea: *Journal of Geophysical Research*, v. 99, p. 15375–15386.
- Green, D.N., and Neuberg, J., 2006, Waveform classification of volcanic low-frequency earthquake swarms and its implication at Soufriere Hills Volcano, Montserrat: *Journal of Volcanology and Geothermal Research*, v. 153, p. 51–63.
- Harlow, D.H., Power, J.A., Laguerta, E.P., Ambubuyog, G., White, R.A., and Hoblitt, R.P., 1994, Precursory seismicity and forecasting of the June 15, 1991, eruption of Mount Pinatubo, *in* Newhall, C.G., and Punongbayan, eds., Fire and mud; eruptions and lahars of Mount Pinatubo, Philippines: Philippine Institute of Volcanology and Seismology and University of Washington Press, p. 285–306.
- Hill, D.P., 1977, A model for earthquake swarms: *Journal of Geophysical Research*, v. 82, no. 8, p. 1347–1352.
- Jacobs, K.M., and McNutt, S.R., 2010, Using seismic *b*-values to interpret seismicity rates and physical processes during the preeruptive earthquake swarm at Augustine Volcano 2005–2006, *in* Power, J.A., Coombs, M.L., and Freymueller, J.T., eds., The 2006 eruption of Augustine Volcano, Alaska: U.S. Geological Survey Professional Paper 1769 (this volume).
- Lahr, J.C., Page, R.A., Chouet, B.A., Stephens, C.D., Harlow, D.H., and others, 1994, Seismic evolution of the 1989–90 eruption sequence of Redoubt Volcano, Alaska: *Journal of Volcanology and Geothermal Research*, v. 62, p. 69–94.
- Langer, H., Falsaperla, S., Powell, T., and Thompson, G., 2006, Automatic classification and a-posteriori analysis of seismic event identification at Soufriere Hills Volcano, Montserrat: *Journal of Volcanology and Geothermal Research*, v. 153, p. 1–10.
- Latter, J.H., 1980, Volcanic earthquakes and their relationship to eruptions at Ruapehu and Ngauruhoe volcanoes: *Journal of Volcanology and Geothermal Research*, v. 9, p. 293–309.
- Minikami, T., 1960, Earthquakes and crustal deformations originating from volcanic activities: *Bulletin of the Earthquake Research Institute*, v. 38, p. 497–544.
- McNutt, S.R., 1996, Seismic monitoring and eruption forecasting of volcanoes; a review of the state-of-the-art and case histories, *in* Scarpa, R., and Tilling, R., eds.,



- Monitoring and mitigation of volcano hazards: Berlin/Heidelberg, Springer-Verlag, p. 99–146.
- McNutt, S.R., 2002, Volcano seismology and monitoring for eruptions, chap. 25 of Lee, W.H.K., Kanamori, H., Jennings, P.C., and Kisslinger, C., eds, *International handbook of earthquake and engineering seismology*: Academic Press, v. 81A.
- Moran, S.C., Malone, S.D., Qamar, A.I., Thelen, W.A., Wright, A.K., and Caplan-Auerbach, J., 2008, Seismicity associated with renewed dome-building at Mount St Helens, 2004–2005, in Sherrod, D.R., Scott, W.E., and Stauffer, P.H., eds., *A volcano rekindled; the renewed eruption of Mount St. Helens, 2004–2006*: U.S. Geological Survey Professional Paper 1750, p.27–60.
- Neuberg, J.W., Tuffen, H., Collier, L., Green, D., Powell, T., and Dingwell, D., 2005, The trigger mechanism of low-frequency earthquakes on Montserrat: *Journal of Volcanology and Geothermal Research*, v. 153, p. 37–50, doi: 10.1016/j.jvolgeores.2005.08.008.
- Patanè, D., Ferrucci, F., and Gresta, S., 1994, Spectral features of microearthquakes in volcanic areas; attenuation in the crust and amplitude response on the site at Mt. Etna, Italy: *Bulletin of the Seismological Society of America*, v. 84, p. 1842–1860.
- Petersen, T., 2007, Swarms of repeating long-period earthquakes at Shishaldin Volcano, Alaska, 2001–2004: *Journal of Volcanology and Geothermal Research*, v. 166, p. 177–192, doi:10.1016/j.jvolgeores.2007.07.014.
- Power, J.A., and Lalla, D.J., 2010, Seismic observations of Augustine Volcano, 1970–2007, in Power, J.A., Coombs, M.L., and Freymueller, J.T., eds., *The 2006 eruption of Augustine Volcano, Alaska*: U.S. Geological Survey Professional Paper 1769 (this volume).
- Rowe, C.A., Thurber, C.H., and White, R.A., 2004, Dome growth behavior at Soufriere Hills Volcano, Montserrat, revealed by relocation of volcanic event swarms, 1995–1996: *Journal of Volcanology and Geothermal Research*, v. 134, no. 3, p. 199–221.
- Rowe, C.A., Aster, R.C., Borchers, B., and Young, C.J., 2002, An automative, adaptive algorithm for refining phase picks in large seismic data sets: *Bulletin of the Seismological Society of America*, v. 92, p. 1660–1674.
- Stephens, C.D., and Chouet, B.A., 2001, Evolution of the December 14, 1989 precursory long-period event swarm at Redoubt Volcano, Alaska: *Journal of Volcanology and Geothermal Research*, v. 109, p. 133–148.
- Thelen, W.A., Crosson, R.S., and Creager, K.C., 2008, Absolute and relative locations of earthquakes at Mount St. Helens, Washington, using continuous data; implications for magmatic processes, in Sherrod, D.R., Scott, W.E., and Stauffer, P.H., eds., *A volcano rekindled; the renewed eruption of Mount St. Helens, 2004–2006*: U.S. Geological Survey Professional Paper 1750, p.71–95.
- Umakoshi, K., Takamura, N., Shinzato, N., Uchida, K., Matsuwo, N., and Shimizu, H., 2008, Seismicity associated with the 1991–1995 dome growth at Unzen Volcano, Japan: *Journal of Volcanology and Geothermal Research*, v. 175, p. 91–99.
- Wallace, K.L., Neal, C.A., and McGimsey, R.G., 2010, Timing, distribution, and character of tephra fall from the 2005–2006 eruption of Augustine Volcano, in Power, J.A., Coombs, M.L., and Freymueller, J.T., eds., *The 2006 eruption of Augustine Volcano, Alaska*: U.S. Geological Survey Professional Paper 1769 (this volume).
- Wilson, C.R., Olson, J.V., Szuberla, C.A.L., McNutt, S., Tytgat, G., and Drob, D.P., 2006, Infrasonic array observations at 153US of the 2006 Augustine Volcano eruptions: *Inframatics*, no. 13, p. 11–26.